Journal of Solid State Chemistry 182 (2009) 1726–1732

Contents lists available at ScienceDirect

Journal of Solid State Chemistry

journal homepage: www.elsevier.com/locate/jssc

Synthesis and characterization of Cr-MSU-1 and its catalytic application for oxidation of styrene

Hong Liu [a,*], Zhigang Wang [a], Hongjiu Hu [b], Yuguang Liang [a], Mengyang Wang [a]

[a] Department of Chemical Engineering, Shanghai University, Shanghai 201800, PR China
[b] College of Science, Shanghai University, Yanchang Road, Shanghai 200072, PR China

ARTICLE INFO

Article history:
Received 11 November 2008
Received in revised form
23 February 2009
Accepted 28 March 2009
Available online 9 April 2009

Keywords:
Cr-MSU-1
Mesoporous molecular sieve
Synthesis
Oxidation of styrene

ABSTRACT

Chromium-containing mesoporous silica material Cr-MSU-1 was synthesized using lauryl alcohol–polyoxyethylene (23) ether as templating agent under the neutral pH condition by two-step method. The sample was characterized by XRD, TEM, FT-IR, UV–Vis, ESR, ICP-AES and N_2 adsorption. Its catalytic performance for oxidation of styrene was studied. Effects of the solvent used, the styrene/H_2O_2 mole ratio and the reaction temperature and time on the oxidation of styrene over the Cr-MSU-1 catalyst were examined. The results indicate that Cr ions have been successfully incorporated into the framework of MSU-1 and the Cr-MSU-1 material has a uniform worm-like holes mesoporous structure. After Cr-MSU-1 is calcined, most of Cr^{3+} is oxidized to Cr^{5+} and Cr^{6+} in tetrahedral coordination and no extra-framework Cr_2O_3 is formed. The Cr-MSU-1 catalyst is highly active for the selective oxidation of styrene and the main reaction products over Cr-MSU-1 are benzaldehyde and phenylacetaldehyde. Its catalytic performance remains stable within five repeated runs and no leaching is noticed for this chromium-based catalyst.

1. Introduction

Since M41S materials were successfully synthesized by Mobil researchers in 1992 [1], many kinds of mesoporous inorganic materials such as FSM-16, SBA, HMS and MSU-*x* have been synthesized by using various types of organic templating agents [2–5]. Among these materials, MSU-*x* is an important family of mesoporous material, which has many advantages. MSU-*x* was characterized by 3D worm-like holes which favor the diffusion of molecular objects. The non-ionic surfactants using as templates in the synthesis of MSU-*x* materials are low-cost, non-toxic and biodegradable. Bagshaw et al. [5] firstly synthesized the mesoporous silica MSU-*x* using non-ionic polyethyleneoxide (PEO)-based templates in neutral pH by a one-step synthesis process. Later, Prouzet et al. [6–8] reported that MSU-*x* silica could be synthesized in a controlled process under mild acidity (pH between 2 and 4), which is a fluoride-assisted two-step synthesis pathway, where the assembly step of silica precursors with micelles can be clearly separated from silica condensation. This new pathway is easier to be adjusted to control the final structure than the one-step method. Pure silica mesoporous materials possess a neutral framework, which limits their application in catalysis. To obtain materials with potential for catalytic applications, it is necessary to modify the nature of the amorphous walls by incorporation of heteroelements. Up to now, a variety of heteroatoms have been reported to incorporate into the framework of MCM-41 and HMS such as Al, Ti, V, Zr, Fe, Co, Cr, Sn, Mn, and so forth [9–11]. However, only little information is available on the synthesis of the heteroatoms substituted MSU-*x* materials [12,13].

Cr is a very important catalytic component for a lot of chemical reactions. In recent years, a series of chromium-containing mesoporous molecular sieves, including Cr-MCM-41 [14], Cr-MCM-48 [15], Cr-HMS [16] and Cr-SBA-1 [17] have received much attention. Lately, Liu and co-workers [13] have prepared the Cr-MSU-1 material using fatty alcohol polyoxyethylene ether ($A(EO)_9$) as the template under acidic conditions by one-step method, but they found the incorporation of chromium into the framework of MSU-1 was very low owing to the high solubility of Cr cations in acidic solution. The similar phenomenon was also observed by Bagshaw et al. [12].

Owing to the acid synthesis pathway does not favor metal incorporation, so in this paper, we expanded the Prouzet's two-step synthesis pathway to neutral pH condition and synthesized the high-quality Cr-MSU-1 using lauryl alcohol polyoxyethylene (23) ether as the template. The chromium-incorporated mesoporous silica material Cr-MSU-1 was characterized by X-ray diffraction (XRD), transmission electron microscopy (TEM), Fourier transform infrared spectroscopy (FT-IR), ultraviolet–visible spectroscopy (UV–Vis), electron spin resonance (ESR), inductively

* Corresponding author. Fax:+86 21 69982828.
E-mail address: liuhong@shu.edu.cn (H. Liu).

0022-4596/$ - see front matter © 2009 Elsevier Inc. All rights reserved.
doi:10.1016/j.jssc.2009.03.033

coupled plasma-atomic emission spectroscopy (ICP-AES) and N_2 adsorption measurements, and its catalytic performance for oxidation of styrene was studied.

2. Experimental

2.1. Synthesis of Cr-MSU-1

Cr-MSU-1 was synthesized under the neutral pH condition using tetraethyl orthosilicate (TEOS) as a silica source, lauryl alcohol-polyoxyethylene (23) ether (Brij35) as a template, respectively. A typical synthesis was performed as follows: 0.576 g of $Cr(NO_3)_3 \cdot 9H_2O$ was added to the Brij35 (5.758 g) solution in water, followed by the addition of 10 g of TEOS dropwise under vigorous stirring. The clear solution remained stirring for 30 min, then 0.081 g NaF was added. The molar composition of mixture was 1.0 SiO_2:0.03 $Cr(NO_3)_3 \cdot 9H_2O$:0.10 Brij35:0.04 NaF:100 H_2O. After the homogeneous gels was aged at ambient temperature under stirring for 24 h, the solid formed was filtered, washed thoroughly with de-ionized water, dried at ambient temperature, and calcined in air at 823 K for 5 h to obtain the Cr-MSU-1 sample.

When the concentration of $Cr(NO_3)_3 \cdot 9H_2O$ was zero in the preparation of Cr-MSU-1 above, the pure silica MSU-1sample was prepared.

The Cr_2O_3/MSU-1 catalyst was prepared by an impregnation method, in which the $Cr(NO_3)_3$ aqueous solution was used as the Cr source. The loading of Cr on MSU-1 was 2.50% (wt) (determined by ICP-AES), and the Cr_2O_3/MSU-1 catalyst was calcined at 823 K for 5 h in air finally.

2.2. Characterization

XRD analysis was performed on a Rigaku D/max-2400 diffractometer using Cu$K\alpha$ radiation and a graphite monochromator. FT-IR spectra were recorded on the Nicolet Nexus 670 FT-IR spectrometer, and the samples to be measured were ground with KBr and pressed into thin wafers. UV–Vis measurements were performed on a Varian Cary-500 spectrometer by using the diffuse reflectance technique in the range of 200–800 nm, and $BaSO_4$ was used as the reference. N_2 adsorption–desorption isotherms were obtained at −196 °C on a Micromeritics ASAP 2010 Sorptometer using static adsorption procedures, and the BET surface areas and pore size distributions were calculated by using N_2 adsorption–desorption isotherms. The TEM images were obtained on a TECNAI 20S-TWIN microscope. Samples for TEM were prepared by dispersing the powdered sample in ethanol by sonication for 20 min and then drop-drying on a copper grid coated with carbon film. ESR spectra were measured at X-band (9 GHz) using a Bruker ER2000D-SRC spectrometer at room temperature. Before the ESR measurement, the sample was dried under vacuum for 4 h at 373 K. The chemical composition of the Cr-MSU-1 sample was analyzed by ICP-AES spectrometry (TJA IRIS1000).

2.3. Oxidation of styrene

The oxidation of styrene was carried out in a three-neck glass flask equipped with a magnetic stirrer and a reflux condenser. In a typical oxidation reaction, 100 mg catalyst were stirred with 2 ml styrene and 10 ml solvent, then 30 wt% H_2O_2 were added to the flask at a given temperature. The reaction temperature and time were varied from 313 to 353 K and from 2 to 7 h, respectively. After reaction, the catalyst was separated from reaction mixture by centrifugation, the reaction products were analyzed by a GC equipped with SE-54 capillary column and a flame ionization detector (FID). The amount of the residual H_2O_2 was determined by iodometric titration.

3. Results and discussion

3.1. Characterization of Cr-MSU-1

The ICP-AES result shown in Table 1 indicates that the Si/Cr ratio in the solid is similar to that in the gel for the Cr-MSU-1 sample. The Cr content in Cr-MSU-1 is 2.45 wt%. This implies that the neutral synthesis condition favors the incorporation of metal ions. The XRD patterns of the calcined Cr-MSU-1, Cr_2O_3/MSU-1 and pure silica MSU-1 materials are shown in Fig. 1. Each sample exhibits only one broad XRD peak at low angle region corresponding to d_{100} reflection. This result clearly indicates that they all have the typical less long-range ordered worm-like mesoporous structure. Compared with the pure silica MSU-1, the impregnation of Cr_2O_3 had no obvious influence to the mesostructure of MSU-1. While the d_{100} diffraction peak of Cr-MSU-1 shifts to lower angle and concurrently the long-range order of MSU-1 diminishes somewhat. The d-spacing of Cr-MSU-1 is higher than that of its pure silica analog (Table 1). This suggests that chromium has been incorporated into the framework of MSU-1. According to the large-angle XRD patterns (Fig. 1b), Cr-MSU-1 does not show any XRD peak of metal oxide. However, the diffraction signals at $2\theta = 24.5^\circ$, 33.6°, 36.2° and 54.8° attributable to the hexagonal phase of Cr_2O_3 (JCPDS No.:84-1616) are observed over the Cr_2O_3/MSU-1 sample.

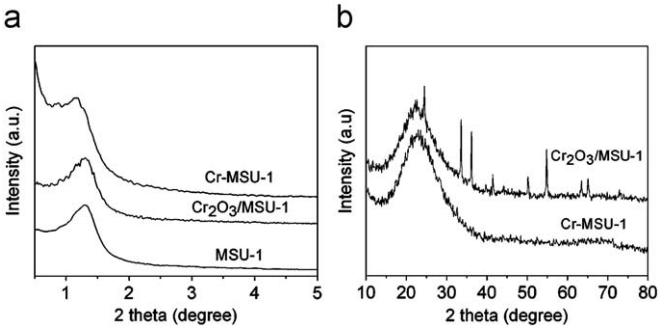

Fig. 1. (a) Small-angle XRD patterns of MSU-1, Cr-MSU-1 and Cr_2O_3/MSU-1 and (b) large-angle XRD patterns of Cr-MSU-1 and Cr_2O_3/MSU-1.

Table 1
Structure properties of MSU-1, Cr-MSU-1 and Cr_2O_3/MSU-1 samples.

Samples	Si/Cr (mol)		Cr content in solid (wt%)	2θ (deg)	d_{100} (nm)	Pore size (nm)	S_{BET} ($m^2 g^{-1}$)	Pore volume ($cm^3 g^{-1}$)
	Gel	Solid						
MSU-1	0	0	0	1.28	6.09	3.2	1107.4	0.98
Cr-MSU-1	33	34	2.45	1.18	6.40	2.8	985.2	0.86
Cr_2O_3/MSU-1			2.50	1.29	6.05	2.7	987.8	0.88

Fig. 2 presents the N_2 adsorption–desorption isotherms and the corresponding BJH pore size distribution curves of Cr-MSU-1, Cr_2O_3/MSU-1 and pure silica MSU-1. A typical type IV isotherm as defined by IUPAC for mesoporous materials are obtained. The abrupt increase in P/P_0 from 0.3 to 0.5 and the maxima in the pore size distribution curves correspond to the uniform mesopores of 2.8, 2.7 and 3.2 nm diameter of Cr-MSU-1, Cr_2O_3/MSU-1 and MSU-1, respectively. The surface area, pore size and pore volume, decrease by the incorporation or impregnation of chromium (Table 1).

Fig. 3 shows FT-IR spectra of MSU-1 and Cr-MSU-1. The IR absorption peaks at 1091, 806 and 461 cm^{-1} are due to the asymmetric and symmetric stretching vibrations as well bending vibration of framework Si–O–Si bonds of MSU-1, respectively [18]. As for Cr-MSU-1 sample, all these absorption peaks shift to low wavenumbers. For instance, the three bands shift to 1082, 802 and 450 cm^{-1}, respectively. In general, this shift of the absorption peaks toward the lower wavenumber is considered an indication of Cr incorporating into the framework of silica tetrahedral [19,20]. The weak absorption peak at 966 cm^{-1} that is observed in the pure silica MSU-1 sample, can be assigned to the stretching vibrations of Si–O in the $Si–O^-–R^+$ groups, that is ν_{as}(Si–OH) presented in the framework of MSU-1. This band is also observed in the FT-IR spectrum of Cr-MSU-1. By carefully examining this band, it is at 966 cm^{-1} in siliceous MSU-1 and is shifted to 956 cm^{-1} in Cr-MSU-1 shown in Fig. 3. The red shift in Cr-MSU-1 implies that Si–OH groups were changed and transformed to the Si–O–Cr bonds [21].

The TEM image of the Cr-MSU-1 sample shown in Fig. 4 reveals a disordered, wormhole mesopore structure as reported by Bagshaw et al. [5]. As shown in Fig. 4, a network of channels is regular in diameter, although long-range packing order is absent.

The UV–Vis diffuse reflectance spectrum for the calcined Cr-MSU-1, given in Fig. 5, shows bands at 250 and 350 nm and a shoulder around 450 nm. The band centered at 450 nm can be assigned to the $^4A_{2g} \rightarrow {}^4T_{1g}$ transition in the octahedral Cr(III) ions [14], implying the presence of unoxidized Cr(III) framework sites even after calcinations. The bands at 250 and 350 nm are usually assigned to O→Cr(VI) and/or Cr(V) charge-transfer absorption bands in tetrahedral environment [14,22,23], indicating that most of chromium is oxidized to Cr(VI) or Cr(V) in tetrahedral coordination after calcination. The existence of chromium in both +5 and +6 oxidation states has been further confirmed by ESR spectroscopy. The absorption band at 600 nm, which is assigned to octahedral Cr(III) in Cr_2O_3 or CrO_x clusters, is not observed in the

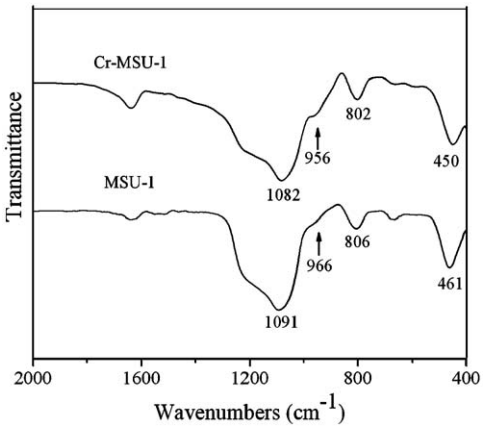

Fig. 3. FT-IR spectra of MSU-1 and Cr-MSU-1.

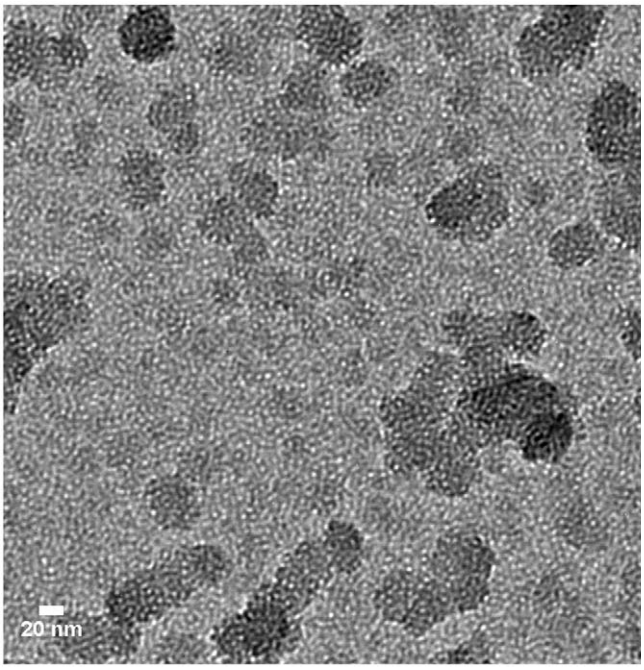

Fig. 4. TEM image of Cr-MSU-1.

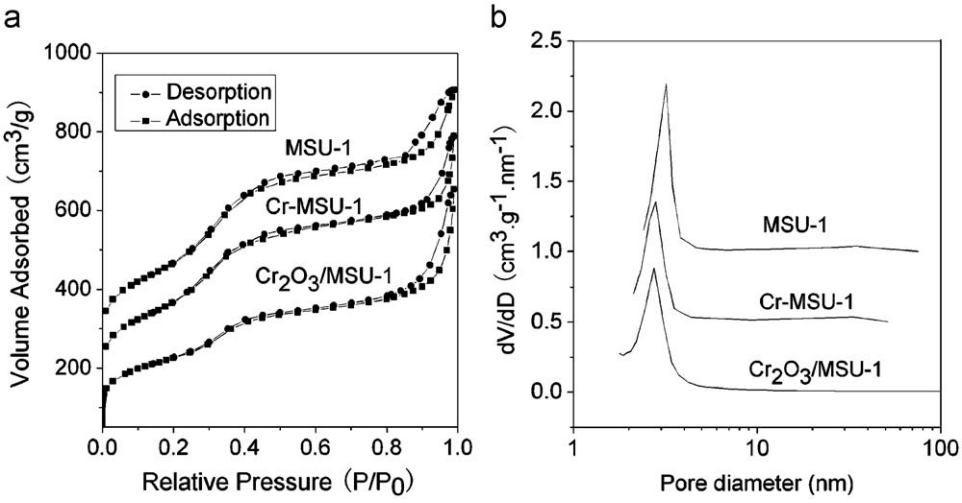

Fig. 2. (a) N_2 adsorption–desorption isotherms and (b) pore size distribution curves of MSU-1, Cr-MSU-1 and Cr_2O_3/MSU-1.

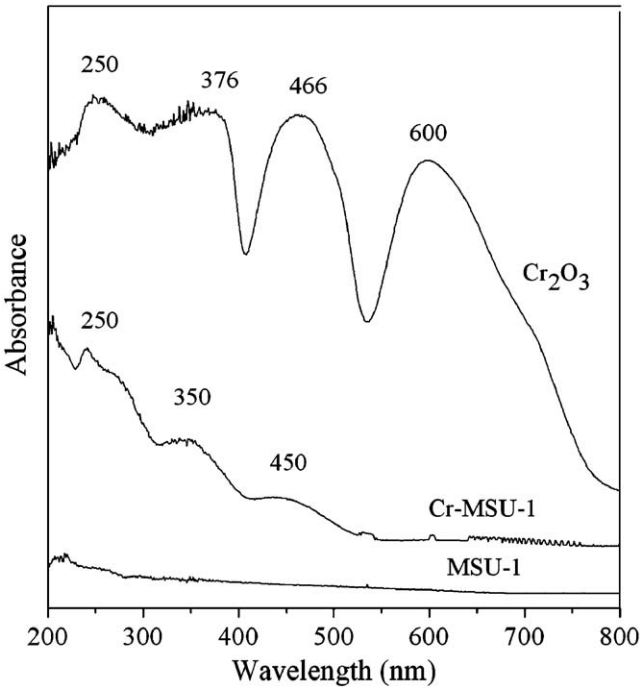

Fig. 5. DR UV–Vis spectra of MSU-1, Cr-MSU-1 and Cr_2O_3.

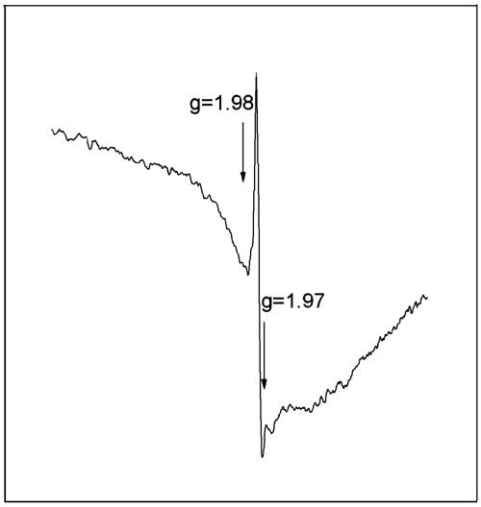

Fig. 6. ESR spectrum of Cr-MSU-1.

calcined Cr-MSU-1. This indicates the absence of extra-framework Cr_2O_3 for the Cr substituted MSU-1 sample.

The ESR spectra of the calcined Cr-MSU-1 show a spectrum with $g_{eff} = 1.98$, indicating the presence of trivalent chromium in octahedral coordination, while for the sample a sharp signal at $g_{eff} = 1.97$ is also observed (Fig. 6), which is characteristic of pentavalent chromium in tetrahedral coordination [14,22]. The Cr(VI) species is diamagnetic [24]. Combining with the DR UV–Vis characterization, it can be concluded that Cr^{3+} ions were oxidized to Cr^{5+} and Cr^{6+} ions after calcinations. The similar results were observed in Cr-MCM-41, where chromium is present as both Cr(V) and Cr(VI) species [14,22,24].

3.2. Catalytic activity of Cr-MSU-1 for oxidation of styrene

Benzaldehyde (BA), phenylacetaldehyde (PA) and styrene oxide (SO), which are important chemical intermediates for the fine chemical industry, are usually the products of the selective oxidation reaction of styrene with H_2O_2 as an oxidant. The process of styrene oxidation in the presence of hydrogen peroxide can be described by reactions included in Scheme 1. We have tested the Cr-MSU-1 material in the catalytic oxidation of styrene with H_2O_2 as an oxidant. The catalytic properties of the Cr-MSU-1 material are presented in Table 2. The results indicate that the pure silica MSU-1 has no activity for oxidation of styrene, which is nearly the same as that of the blank test. However, Cr-MSU-1 reveals a high catalytic activity, which is obviously superior to that of the Cr_2O_3 supported on MSU-1 catalyst (Cr_2O_3/MSU-1). Their activity difference arises from the different coordination environments of Cr species in the samples. The Cr species in Cr-MSU-1 locate at isolated tetrahedral coordinated sites rather than becoming aggregated Cr_2O_3 clusters in the case of Cr_2O_3/MSU-1 (confirmed by XRD in Fig. 1), and they are responsible for the high catalytic activity for the styrene oxidation. Compared to TS-1, Cr-MSU-1 is more active for styrene oxidation. This may be due to the channel advantage of the Cr-MSU-1. It should be noted that phenylaldehyde is the main product when using TS-1 as catalyst [25], the main reaction product over Cr-MSU-1 catalyst is benzaldehyde, followed by phenylacetaldehyde and styrene oxide, and a small amount of styrene glycol and benzoic acid has also been identified possibly because the reaction mechanism differs in different catalysts. The high selectivity for benzaldehyde over Cr-MSU-1 catalyst is consistent with spinel-type $Mg_xFe_{3-x}O_4$ and other metal-substituted mesoporous catalysts [15,26,27].

The nature of solvent has an important effect on the outcome of the reaction. In order to investigate the solvent effect in the styrene oxidation, we have used both aprotic and protic solvents such as: acetonitrile, acetone, methanol, ethanol, isopropanol and *n*-butanol. The effect of different solvents on styrene conversion and product selectivity over Cr-MSU-1 are summarized in Table 3. For both protic and aprotic solvents, as the polarity of the solvent increases (e.g. *n*-butanol < isopropanol = ethanol < methanol; acetone < acetonitrile), the conversion of styrene and H_2O_2 as well as the utilization for benzaldehyde and phenylacetaldehyde decreases. It can be caused by competitive absorption of solvent and hydrogen peroxide on the surface of catalyst. By the increasing solvent polarity, solvent will be more easily adsorbed in the active site of catalyst than the hydrogen peroxide, thus reducing the styrene conversion and H_2O_2 utilization. Furthermore, when aprotic acetone or acetonitrile as solvent, the selectivity for by-products (styrene glycol, styrene monoether and benzoic acid) is obviously lower than that in alcoholic protic solvents. We can explain these results taking into account the competitions between the reactions depicted in Scheme 1. When alcohol is used as solvent, the reaction (2) becomes a strong competitor of the reaction (1) and reaction (3), leading to the high selectivity to styrene glycol and styrene monoether. In addition, the type of ROH has also influence on the product distribution of styrene oxide. Compared with isopropanol or *n*-butanol, methanol is more polar and hydrophilic and has less molecule volume, which can more easily penetrate and form styrene glycol and styrene monoether, thus the selectivity to BA and PA reduces. Contrarily, the formation of the corresponding styrene glycol and monoether is hindered in bulky alcoholic solvents. Accordingly, the high selectivity to BA and PA is achieved in the presence of these alcohols.

The influence of styrene/H_2O_2 molar ratio on the styrene conversion and product distribution is given in Table 4. With the decrease in styrene/H_2O_2 molar ratio, the styrene conversion increases from 15.6% to 29.5% at the cost of H_2O_2 utilization. The selectivity for benzaldehyde increases along with the growing amount of by-products such as styrene glycol and benzoic acid, indicating that excess amount of H_2O_2 favors the oxidation

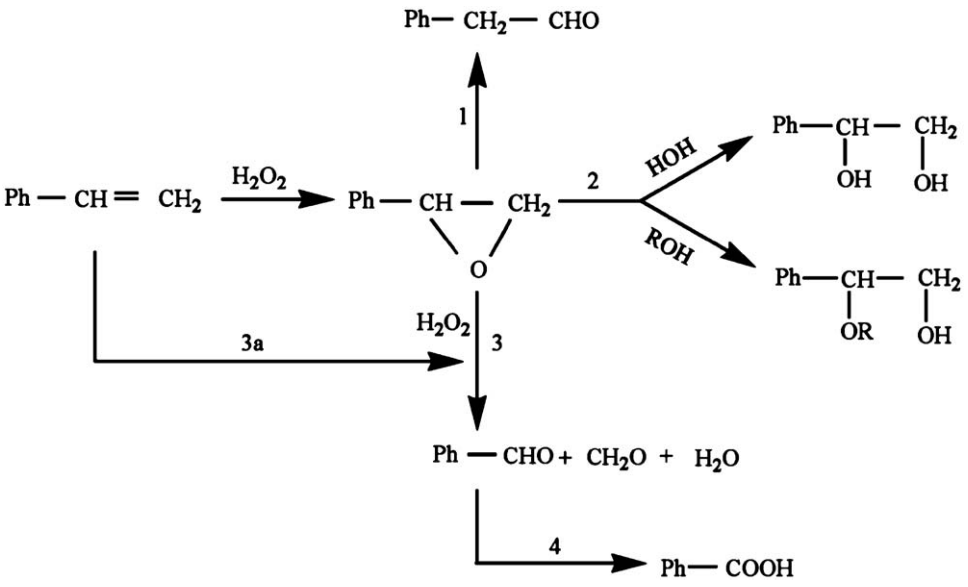

Scheme 1. Reaction routes of styrene oxidation.

Table 2
Catalytic performances of the catalysts for the oxidation of styrene.

Catalyst	X(Styrene) (%)	$X(H_2O_2)$ (%)	$U(H_2O_2)$ (%)	Selectivity (%)			
				BA	SO	PA	Others
Blank test	0	75.2	0	0	0	0	0
MSU-1	0	72.6	0	0	0	0	0
Cr-MSU-1	23.6	96.4	70.7	60.2	4.9	30.6	4.3
Cr_2O_3/MSU-1	4.36	92.3	13.1	60.4	6.6	24.1	8.9
TS-1(Si/Ti = 43)[a]	13.9	–	82.4	12.6	9.4	63.5	14.5

Reaction conditions: m(catalyst)/m(styrene) = 5.0%, n(styrene)/$n(H_2O_2)$ = 3, T = 333 K, t = 3 h, solvent: acetone.
X(Styrene), $X(H_2O_2)$, $U(H_2O_2)$—styrene conversion, H_2O_2 conversion and utilization, respectively.
BA—benzaldehyde, SO—styrene epoxide, PA—phenylacetaldehyde, Others—styrene glycol, styrene monoether and benzoic acid.
[a] Condition from Ref. [25]: n(styrene)/$n(H_2O_2)$ = 2, T = 343 K, t = 5 h, solvent: acetone.

Table 3
Effect of the solvents on the oxidation of styrene over Cr-MSU-1.

Solvent	X(Styrene) (%)	$X(H_2O_2)$ (%)	$U(H_2O_2)$ (%)	Selectivity (%)			
				BA	SO	PA	Others
Methanol	22.4	98.1	67.2	50.1	0.7	6.5	42.8
Ethanol	24.0	97.6	72.1	76.1	1.7	4.9	17.3
Isopropanol	24.4	99.1	73.3	73.9	3.8	10.1	12.2
n-Butanol	26.1	99.7	78.3	69.6	4.1	17.0	9.3
Acetonitrile	16.7	88.9	50.1	83.1	1.9	7.1	7.9
Acetone	23.6	96.4	70.7	60.2	4.9	30.6	4.3

Reaction conditions are same as Table 2.

Table 4
Effect of styrene/H_2O_2 molar ratio on the oxidation of styrene over Cr-MSU-1.

n(Styrene)/$n(H_2O_2)$	X(Styrene) (%)	$X(H_2O_2)$ (%)	$U(H_2O_2)$ (%)	Selectivity (%)			
				BA	SO	PA	Others
1	29.5	85.6	29.6	78.5	1.8	5.1	14.6
2	24.4	92.4	48.7	66.3	4.7	21.4	7.6
3	23.6	96.4	70.7	60.2	4.9	30.6	4.3
4	20.5	98.6	82.1	47.2	4.6	45.6	2.5
5	15.6	99.2	78.1	46.7	4.7	46.5	2.1

Reaction conditions: m(catalyst)/m(styrene) = 5%, T = 333 K, t = 3 h, solvent: acetone.

cleavage of C=C to transfer into benzaldehyde and the formation of styrene glycol and benzoic acid from styrene oxide, respectively. The styrene/H_2O_2 molar ratio of 3 is proved proper from Table 4.

The effect of reaction temperature on the styrene conversion and product distribution is shown in Table 5. As expected, by increasing reaction temperature from 313 to 333 K, styrene conversion increases from 5.55% to 23.6%, along with the increasing of H_2O_2 conversion and utilization. However, a further increase in the temperature to 353 K exhibits a decrease of styrene conversion and H_2O_2 utilization, which are mostly due to the decomposition of hydrogen peroxide at this reaction temperature. In addition, as the reaction temperature increases the selectivity towards benzaldehyde decreases and selectivity for epoxidation products (SO, PA, styrene glycol and styrene monoether et al.) are improved. This confirms that the cleavage of C=C is higher at lower temperature and the epoxidation competes more favorably against C=C cleavage at higher temperature [26]. As seen from Table 5, the optimum reaction temperature is 333 K.

The effect of reaction time on styrene conversion and product distribution is given in Table 6. As expected, styrene conversion increases with reaction time, together with the increasing H_2O_2 conversion and utilization. The selectivity for benzaldehyde remains almost unchanged. However, too prolonged reaction time favors a large amount of styrene glycol and benzoic acid. The optimum reaction time is 3–6 h.

The catalytic stability of the Cr-MSU-1 sample was further explored under one protic and one aprotic solvent, i.e. *n*-butanol and acetone. The reactant composition was kept at the level of: styrene/H_2O_2 = 3 (mol/mol), catalyst/styrene = 1/20 (g/g) and solvent/styrene = 1 (ml/ml). The reaction was conducted at 333 K for 7 h for each run. After one run, the catalyst was regenerated by washing with fresh acetone or *n*-butanol for three times. Table 7 shows that within five recycles, the activity and selectivity of the Cr-MSU-1 catalyst remains nearly the same. This indicates that the Cr-MSU-1 molecular sieve is a reusable catalyst and no leaching of chromium ions from the matrix, which can be attributed to the absence of non-framework chromium ions in the matrix. No change of chromium content after five recycles can be further confirmed by ICP–AES results as shown in Table 8. However, for the impregnated Cr_2O_3/MSU-1 catalyst, the loss of chromium ions reaches to 39.6% and 40.8% after five recycles in acetone and *n*-butanol, respectively. It is attributed to the non-framework Cr cations in Cr_2O_3/MSU-1, resulting in the leaching of Cr during reaction.

4. Conclusions

Cr-MSU-1 was successfully synthesized using lauryl alcohol–polyoxyethylene (23) ether as templating agent under the neutral pH condition. The characterization results show that the Cr-MSU-1 material has a uniform 3D worm-like holes mesostructure. After calcined, most of Cr^{3+} is oxidized to Cr^{5+} and Cr^{6+} in tetrahedral

Table 7
Catalytic stability of the Cr-MSU-1 sample.

Condition	*X*(Styrene) (%)	Selectivity (%)			
		BA	SO	PA	Others
Acetone					
First run	29.1	60.9	3.8	25.8	9.5
Second run	30.3	61.5	3.7	26.3	8.5
Third run	28.9	60.5	3.4	27.3	8.8
Fourth run	29.5	61.9	4.6	25.4	8.1
Fifth run	29.0	62.1	4.1	26.1	7.7
n-Butanol					
First run	32.1	70.5	3.9	13.2	12.4
Second run	32.6	71.2	4.2	12.7	11.9
Third run	31.7	70.1	4.0	13.1	12.8
Fourth run	30.3	69.5	3.8	13.5	13.2
Fifth run	30.5	68.9	3.2	14.1	13.8

Reaction conditions: m(catalyst)/m(styrene) = 5.0%, n(styrene)/n(H_2O_2) = 3, T = 333 K, t = 7 h.

Table 5
Effect of the reaction temperature on the oxidation of styrene over Cr-MSU-1.

Temperature (K)	*X*(Styrene) (%)	*X*(H_2O_2) (%)	*U*(H_2O_2) (%)	Selectivity (%)			
				BA	SO	PA	Others
313	5.55	88.7	16.7	83.3	3.2	12.8	0.7
323	16.9	91.2	50.6	82.6	1.9	13.5	2.0
333	23.6	96.4	70.7	60.2	4.9	30.6	4.3
343	20.4	99.2	61.2	57.1	1.2	24.6	17.1
353	19.5	99.7	58.5	50.8	3.3	27.5	18.4

Reaction conditions: m(catalyst)/m(styrene) = 5.0%, n(styrene)/n(H_2O_2) = 3, t = 3 h, solvent: acetone.

Table 6
Effect of the reaction time on the oxidation of styrene over Cr-MSU-1.

Time (h)	*X*(Styrene) (%)	*X*(H_2O_2) (%)	*U*(H_2O_2) (%)	Selectivity (%)			
				BA	SO	PA	Others
2	17.8	85.2	53.3	63.1	5.3	28.7	2.9
3	23.6	96.4	70.7	60.2	4.9	30.6	4.3
4	24.1	97.2	72.2	63.8	4.9	25.7	5.6
5	25.4	97.4	76.3	63.7	5.1	25.1	6.1
6	28.4	98.6	85.1	60.3	4.6	27.8	7.3
7	29.1	99.2	87.4	60.9	3.8	25.8	9.5

Reaction conditions: m(catalyst)/m(styrene) = 5.0%, n(styrene)/n(H_2O_2) = 3, T = 333 K, solvent: acetone.

Table 8
ICP-AES data of the Cr-MSU-1 and Cr_2O_3/MSU-1 sample before and after five reaction recycles.

Sample	Before	After		Loss caused by leaching (%)	
	Cr content (wt%)	Cr content (wt%)	Cr content (wt%)		
Cr-MSU-1	2.45	2.39[a]	2.41[b]	2.45[a]	1.63[b]
Cr_2O_3/MSU-1	2.50	1.51[a]	1.48[b]	39.6[a]	40.8[b]

[a] Acetone as solvent.
[b] *n*-Butanol as solvent.

coordination and no extra-framework Cr_2O_3 is formed. The Cr-MSU-1 catalyst reveals an exceptional catalytic activity for the oxidation of styrene. The reaction conditions, including solvent, styrene/H_2O_2 ratio, reaction temperature and reaction time, have a strong influence on the catalytic performances. The Cr-MSU-1 material is stable to retain its activity and selectivity at least for five repeated runs and no leaching of chromium ions from the matrix is found.

Acknowledgments

This study is supported financially by Shanghai Municipal Commission of Education (Grant no. 06AZ058) and Shanghai Leading Academic Disciplines (no. S30109; no. Y0103).

References

[1] C.T. Kresge, M.E. Leonowicz, W.J. Roth, J.C. Vartuli, J.S. Beck, Nature 359 (1992) 710–712.
[2] S. Inagaki, Y. Fukushima, K. Kuroda, Chem. Commun. (1993) 680–681.
[3] D. Zhao, J. Feng, Q. Huo, N. Melosh, G.H. Fredrickson, B.F. Chmelka, G.D. Stucky, Science 279 (1998) 548–552.
[4] T.R. Pauly, T.J. Pinnavaia, Chem. Mater. 13 (2001) 987–993.
[5] S.A. Bagshaw, É. Prouzet, T.J. Pinnavaia, Science 269 (1995) 1242–1244.
[6] C. Boissière, A. Van der Lee, A. El Mansouri, A. Larbot, É. Prouzet, Chem. Commun. (1999) 2047–2048.
[7] C. Boissière, A. Larbot, A. Van der Lee, P.J. Kooyman, É. Prouzet, Chem. Mater. 12 (2000) 2902–2913.
[8] C. Boissière, A. Larbot, É. Prouzet, Chem. Mater. 12 (2000) 1937–1940.
[9] L. Norena-Franco, I. Hernandez-Perez, J. Aguilar-Pilego, A. Maubert-Franco, Catal. Today 75 (2002) 189–195.
[10] K. Chaudhari, T.K. Das, P.R. Rajmohanan, K. Lazar, S. Sivasanker, A.J. Chandwadkar, J. Catal. 183 (1999) 281–291.
[11] H. Liu, G. Lu, Y. Guo, Y. Guo, J. Wang, Nanotechnology 17 (2006) 997–1003.
[12] S.A. Bagshaw, T. Kemmitt, N.B. Milestone, Microporous Mesoporous Mater. 22 (1998) 419–433.
[13] L. Liu, H. Li, Y. Zhang, J. Phys. Chem. B 110 (2006) 15478–15485.
[14] A. Sakthivel, P. Selvam, J. Catal. 211 (2002) 134–143.
[15] S. Gómez, L.J. Garces, J. Villegas, R. Ghosh, O. Giraldo, S.L. Suib, J. Catal. 233 (2005) 60–67.
[16] H. Yamashita, K. Yoshizawa, M. Ariyuki, S. Higashimoto, M. Che, M. Anpo, Chem. Commun. (2001) 435–436.
[17] X. Zhao, X. Wang, J. Mol. Catal. A 261 (2007) 225–231.
[18] M.D. Alba, Z. Luan, J. Klinowski, J. Phys. Chem. 100 (1996) 2178–2182.
[19] M.D. Kadgaonkar, S.C. Laha, P. Kumar, S.P. Mirajkar, R. Kuma, Catal. Today 97 (2004) 225–231.
[20] S.C. Laha, P. Mukherjee, S.R. Sainkar, R. Kumar, J. Catal. 207 (2002) 213–223.
[21] M. Jang, J.K. Park, E.W. Shin, Microporous Mesoporous Mater. 75 (2004) 159–168.
[22] Z. Zhu, Z. Chang, L. Kevan, J. Phys. Chem. B 103 (1999) 2680–2688.
[23] B.M. Weckhuysen, A.A. Verberckmoes, A.R. De Baets, R.A. Schoonheydt, J. Catal. 166 (1997) 160–171.
[24] Z. Yuan, J. Wang, Z. Zhang, T. Chen, H. Li, Microporous Mesoporous Mater. 43 (2001) 227–236.
[25] V. Huleaa, E. Dumitriu, Appl. Catal. A 277 (2004) 99–106.
[26] N. Ma, Y. Yue, W. Hua, Z. Gao, Appl. Catal. A 251 (2003) 39–47.
[27] L. Zhang, Z. Hua, X. Dong, L. Li, H. Chen, J. Shi, J. Mol. Catal. A 268 (2007) 155–162.